

A Simple Light Isotope Metabolic Labeling (SLIM-labeling) Strategy: A Powerful Tool to Address the Dynamics of Proteome Variations *In Vivo**[§]

Thibaut Léger[‡], Camille Garcia[‡], Laetitia Collomb[‡], and Jean-Michel Camadro^{‡§¶}

Many quantitative proteomics strategies rely on *in vivo* metabolic incorporation of amino acids with modified stable isotope profiles into proteins. These methods give rise to multiple ions for each peptide, with possible distortion of the isotopolog distribution, making the overall analytical process complex. We validated an alternative strategy, simple light isotope metabolic labeling (SLIM-labeling), which alleviates many of these problems. SLIM-labeling is based on the *in vivo* reduction of the isotopic composition of proteins using metabolic precursors with a unique light isotope composition to label all amino acids. This brings a new dimension to in-depth, high resolution MS-based quantitative proteomics. Here, we describe a ¹²C-based SLIM-labeling strategy using U-[¹²C]-glucose as the metabolic precursor of all amino acids in the pathogenic yeast *Candida albicans*. Monoisotopic ion intensity increased exponentially following ¹²C enrichment, substantially improving peptide identification scores and protein sequence coverage in bottom-up analyses. Multiplexing samples of ¹²C composition varying from natural abundance (98.93%) to 100% makes it possible to address relative quantification issues, keeping all the critical information for each peptide within a single isotopolog cluster. We applied this method to measure, for the first time, protein turnover at the proteome scale in *Candida albicans* and its modulation by inhibitors of the proteasome and vacuolar protein degradation systems. *Molecular & Cellular Proteomics* 16: 10.1074/mcp.M117.066936, 2017–2031, 2017.

The fundamental process in MS-based bottom-up proteomics is to extract information on the mass, charge, and

intensity of every peptide ion detected in typical LC-MS runs. Peptide ions are composed of a series of isotopologs because of the presence of naturally occurring stable isotopes of the common elements. The relative abundance of each isotopolog within the isotope cluster is dependent on peptide length and sequence. Peptide identification relies both on the precise estimation of the mass of the precursor ion, obtained after deisotoping (determination of the monoisotopic mass) of the isotope cluster, and interpretation of the MS/MS fragmentation pattern. Most quantitative proteomics analyses use *in vivo* metabolic labeling strategies to introduce isotopically labeled amino acids into proteins. They may be provided in rich growth media containing ²H (1), ¹⁵N (2), or ¹³C (3) labeled amino acid precursors or supplied as individual reagents in defined media (SILAC (4) and derived methods (5, 6), reviewed in (7)). Matching the labeled and unlabeled peaks for ¹⁵N or ¹³C labeling methods can be challenging, because the mass shift is variable and depends on the total number of atoms (N or C, respectively) in the selected peptides. This problem does not occur in SILAC experiments, in which incorporation of labeled arginine and/or lysine combined with the use of trypsin, Lys-C or Lys-N (8) for digestion, is associated with a fixed mass shift between labeled and unlabeled peptides. Despite better experimental reproducibility relative to, for example, label-free quantification procedures, SILAC suffers from lower identification efficiencies (9). This is because of the greater number of experimental ions to be analyzed and associated ion suppression, which needs to be compensated by sample fractionation before LC-MS analyses (10).

In a series of seminal papers (11–13), the group of Alan Marshall reported that reducing the isotope complexity of proteins leads to significant improvement in the determination of their monoisotopic mass when analyzed on FT-ICR mass spectrometers. Theoretical models (14) have suggested that this result is because of an improved signal-to-noise ratio. This approach remained largely ignored by the proteomics community, possibly because of limited access to FT-ICR MS facilities. The recent advances in high resolution, high sensitivity mass spectrometers may provide the appropriate tools to fully exploit the benefits of reducing the isotope complexity

From the [‡]Mass Spectrometry Laboratory, Institut Jacques Monod, UMR 7592, Univ Paris Diderot, CNRS, Sorbonne Paris Cité, F-75205 Paris Cedex 13, France; [§]Mitochondria, Metals, and Oxidative Stress Group, Institut Jacques Monod, UMR 7592, Univ Paris Diderot, CNRS, Sorbonne Paris Cité, F-75205 Paris Cedex 13, France

Received January 4, 2017, and in revised form, July 19, 2017

Published, MCP Papers in Press, August 18, 2017, DOI 10.1074/mcp.M117.066936

Author contributions: T.L. and J.M.C. designed research; T.L., C.G., L.C., and J.M.C. performed research; T.L., C.G., L.C., and J.M.C. analyzed data; T.L. and J.M.C. wrote the paper.

of proteins by using a U- ^{12}C labeling strategy to address both the in-depth analysis of complex proteomes and their dynamics. We provide a proof-of-concept of the added value of reducing isotope complexity *in vivo* by performing bottom-up proteomic analyses of a simple eukaryotic unicellular organism, the pathogenic yeast *Candida albicans*, grown on a synthetic medium containing either U- ^{12}C -glucose or natural glucose as the sole carbon source. Glucose catabolism allows the biosynthesis of all amino acids *in vivo*. Comparison of the datasets showed a remarkable improvement in protein identifications, scores, and sequence coverages when the isotopic complexity was reduced *in vivo*.

Mixing samples from both growth conditions opens the way to a new quantitative proteomics method. Quantitative variations of peptide abundances can be easily measured by analyzing the ratio between the monoisotopic ion to the sum of all isopologs intensities for every peptide in the mixture. Among the many possible applications of this alternative to SILAC-based quantitative proteomics, we chose to demonstrate the power of this new method in one of the most challenging problems in quantitative proteomics, the evaluation of protein half-lives *in vivo*. Time course experiments after shifting cells from one glucose-specific growth medium to another allowed us to experimentally determine the turnover of thousands of proteins, and the perturbations induced by adding either MG132 (N-Benzoyloxycarbonyl-L-leucyl-L-leucyl-L-leucinal), an inhibitor of the proteasomal protein-degradation machinery (15), or PMSF (phenylmethylsulfonyl fluoride)¹, a general serine-protease inhibitor that more specifically targets vacuolar proteases in yeast (16), to the growth medium. A key step in the analytic process is to extract ^{12}C abundance from the isotope clusters for each peptide. Here we show that the experimental isotope clusters fit remarkably well with the theoretical clusters computed using the MIDAS webserver at the NCBI (<http://www.ncbi.nlm.nih.gov/CBBresearch/qmbp/midas/index.html>) (17), making it possible to generate high quality calibration standards for ^{12}C enrichment measurements. We believe that this strategy for *in vivo* protein labeling may contribute significantly to the development of new approaches to explore key features of proteome dynamics.

MATERIALS AND METHODS

Strains and growth conditions—The *C. albicans* strain SC5314 (18) was grown on a defined synthetic medium (Yeast Nitrogen Base) with glucose (0.5% w/v) as the sole source of carbon. Cells were grown in two types of culture conditions, using either regular glucose (N-G), or glucose containing only ^{12}C carbon atoms (U- ^{12}C -glucose, Euriso-Top, Saint-Aubin, France; filter sterilized) (^{12}C -G). The carbon isotopic composition of N-G is 98.93% ^{12}C , 1.07% ^{13}C . Cell cultures (100 ml) were inoculated at an initial OD_{600} of 0.1 with liquid pre-

cultures (10 ml of the same medium inoculated with freshly grown colonies on YPD agar plates) and incubated in an orbital shaker at 30 °C. In the labeling experiments, the cells grown in YNG-N-G medium were collected in the mid-exponential growth phase ($\text{OD}_{600} = 2$) by centrifugation (3 min at $3000 \times g$) and transferred to fresh YNB medium containing 0.5% ^{12}C -G. When a chemical treatment was applied to the cells, the cultures were exposed to the drug for 3 min before the centrifugation step, and then resuspended in fresh medium containing the same final concentration of the drug (1 mM PMSF, 10 μM MG132, both from 1000X stock solutions in DMSO) in an equal volume of DMSO (0.1% v/v final concentration). For time-course experiments, the cells were collected by centrifugation (3 min at $3000 \times g$) 15, 30, 60, 120, and 240 min after introduction of the drug from cultures with characteristic doubling times of 2.85 (control), 2.75 (MG132), and 4.33 h, (PMSF) ($n = 3$) (supplemental Fig. S8). The cell pellets were immediately frozen and stored at -80°C until processed for protein extraction using the Yeast Protein Extraction Kit (Expedeon, San Diego, CA, USA) and further proteomic analysis. *C. albicans* grew as budding-yeast under the conditions tested. Crude lysates (20 μg per condition) were digested with trypsin (12.5 $\mu\text{g}/\text{ml}$; Promega, Madison, WI), according to the FASP protocol (Expedeon).

LC-MS/MS Acquisition—We analyzed 2 μg of protein digests from crude samples from the different cell conditions in triplicate with an Orbitrap Fusion Tribrid, coupled to a Nano-LC Proxeon 1000, equipped with an easy spray ion source (all from Thermo Scientific). Peptides were separated by chromatography with the following parameters: Acclaim PepMap100 C₁₈ pre-column (2 cm, 75 μm i.d., 3 μm , 100 Å), Pepmap-RSLC Proxeon C₁₈ column (50 cm, 75 μm i.d., 2 μm , 100 Å), 300 nL/min flow rate, gradient from 95% solvent A (water, 0.1% formic acid) to 35% solvent B (100% acetonitrile, 0.1% formic acid) over a period of 127 min, followed by column regeneration for 23 min, giving a total run time of 2.5 h. Peptides were analyzed in the Orbitrap cell, in full ion scan mode, at a resolution of 120,000 (at m/z 200), with a mass range of m/z 350–1550 and an AGC target of 2×10^5 . Fragments were obtained by higher-energy C-trap dissociation (HCD) activation with a collisional energy of 30%, and a quadrupole isolation window of 1.6 Da. MS/MS data were acquired in the ion trap in top-speed mode, with a total cycle of 3 s, with an AGC target of 5×10^4 , a dynamic exclusion of 50 s and an exclusion duration of 60 s. Precursor priority was given to the most intense peptides. Peptides with charge states from 2 to 8 were selected for MS/MS acquisition. The maximum ion accumulation times were set to 250 ms for MS acquisition and 30 ms for MS/MS acquisition in parallelization mode. All MS and MS/MS data for protein samples were processed with Proteome Discoverer software (Thermo Scientific, version 2.1) and the Mascot search engine (Matrix Science, version 5.1). The mass tolerance was set to 7 ppm for precursor ions and 0.5 Da for fragments. The following

¹ The abbreviations used are: PMSF, phenylmethylsulfonyl fluoride; HCD, higher-energy C-trap dissociation.

variable modifications (2 maximum per peptide) were allowed: oxidation (M), phosphorylation (ST), Gly-Gly (K), Leu-Arg-Gly-Gly (K), carbamidomethylation (C). The maximum number of missed cleavages was limited to two for the trypsin protease (specificity Lys or Arg except Lys-Pro and Arg-Pro). MS/MS data were used to search an extraction of the diploid *C. albicans* ORF database (*C_albicans_SC5314_A22_current_orf_trans_all.fasta*, 12,277 entries, 03–27–2016) retrieved from the Candida Genome Database website (19) (<http://www.candidagenome.org/>). Our database contained all the protein sequences from one allele (arbitrary chosen as allele A; 6209 entries), those encoded by mitochondrial DNA (17 entries), and pseudo-sequences of proteins obtained for all polymorphic alleles by aggregating the tryptic peptides computed to be specific for the second allele (allele B, 3236 entries). We deposited the resulting database (9462 entries) in the Pride repository. Peptide identifications were validated using a 1% FDR (False Discovery Rate) threshold calculated with the Percolator algorithm.

Quantitative Analysis of Proteins and Peptides from the Different Data Sets in Label-free Experiments—The abundance of peptides obtained for all time points were normalized using Progenesis for proteomics software (Nonlinear Dynamics Ltd., Newcastle, UK). The mass tolerance was set to 7 ppm for precursor ions and 0.5 Da for fragments. The normalized abundance of proteins with similar normalized abundance differences (ANOVA *p* value < 0.05) were classified together by the AutoClass Bayesian clustering system (web-server Autoclass@IJM, <http://ytat2.ijm.univ-paris-diderot.fr/>) (20) and visualized with Javatreeview (<http://jtreeview.sourceforge.net/>). Between-subject analyses were carried out on the various data sets.

Simulation of Peptide Isotopolog Distribution and Intensity—Considering that the general elemental composition of most peptides/proteins is in the form, $C_vH_wN_xO_yS_z$, we used the polynomial approximation of the monoisotopic ion abundance (*P*) given by $p = \text{Pr}(^{12}\text{C})^v \cdot \text{Pr}(^1\text{H})^w \cdot \text{Pr}(^{14}\text{N})^x \cdot \text{Pr}(^{16}\text{O})^y \cdot \text{Pr}(^{32}\text{S})^z$, where $\text{Pr}(^i\text{X})$ represents the natural abundance, or probability of occurrence, of a particular isotope of the element X present in the formula (for a review, see (21)). The theoretical MS spectra were computed using Molecular Isotopic Distribution Analysis (MIDAS) software (17). The MIDAS algorithm used a “polynomial-based method” to compute theoretical spectra, and a 0.01 Da mass accuracy to compute their fine-grained isotopic distribution. The mass/intensity of each simulated MS spectrum was exported for further processing.

LC-MS/MS Data Processing—The LC-MS/MS.raw files were processed using (i) the Mascot search engine coupled to Proteome Discoverer 2.1 for peptide identification and (ii) Progenesis Q1 for metabolomics to extract the abundance of the isotopologs of all isotope clusters. The resulting data files were matched according to the neutral mass and retention time of identified peptides, and merged. We computed the

ratio (R_{iso}) of the abundance of the monoisotopic ion over the total isotopolog cluster for each identified peptide. This ratio reflects the amount of ^{12}C incorporated into the peptides. We experimentally defined a standard calibration curve by mixing known amounts of protein extracts from YNB-N-G and YNB- ^{12}C -G cultures. We compared the ratio extracted from the experimental data to the theoretical ratio computed for each peptide using the MIDAS application, according to the carbon composition used in the different points of the calibration curve (1.07%-[^{13}C] (natural abundance), 25%-[^{12}C], 50%-[^{12}C], 75%-[^{12}C], and 100%-[^{12}C]). We used the slope of the linear correlation curve between MIDAS *versus* experimental ratios to normalize the experimental values. We excluded all experimental ratios of peptides (for each time point) that varied by more than 20% relative to theoretical values. The ^{12}C incorporation law described by the equation $y = k \cdot e^{ax}$ was determined from the experimental ratio for each calibration point with *y* representing the abundance ratio of the monoisotopic mass on the sum of the abundance of all isotopologs and *a* the amount of ^{12}C in each peptide. Only peptides presenting at least three ^{12}C incorporation values of the five calibration points were considered further. Equations for 20,261 peptides (corresponding to 3363 proteins) were determined with an averaged R^2 of 0.981.

Computational Methods for Determining Protein Turnover—Protein turnover was determined in time-course labeling experiments in which the cells were transferred from YNB-N-G medium, providing “heavy” proteins, to YNB- ^{12}C -G medium, in which the newly synthesized proteins were of the “light” type. We computed the ^{12}C enrichment (and therefore the *r* values) for each peptide as described above, except that we independently used either the experimental or the MIDAS-based calibration curves. The overall ^{12}C incorporation into each protein was calculated by averaging the values obtained for its individual peptides, excluding outliers defined as those that differed by more than one standard deviation from the mean incorporation in a peptide group. Peptides with different charge states were treated as different entries for the determination of ^{12}C composition. The experimental light/heavy protein composition ratio increased according to an exponential model of ^{12}C incorporation. We computed the best linear fit of the natural log transformation of the ratio over time and the carbon composition of the peptide was validated if the resulting R^2 was higher than 0.9 in curves with at least three or four of the five time points. The protein turnover ($T_{1/2}$) calculation takes into account the degradation rate (*k*) of the protein and the growth rate ($\ln 2/\text{doubling time} = \mu$) of the cells, using the same formalism as that described by Larrabee *et al.* (20). The degradation rate *k* is obtained by subtracting μ to the slope of the natural log transform of (*r*+1) plotted over the *m* time points. The rate constant of the protein decay was calculated following the equations (22) for the exponential model that was developed as follows:

We considered the protein at any time P_t to be a function of the protein at t_0 , the time corresponding to the shift of the cells from normal glucose to U- ^{12}C -glucose containing media. By convention, we denote the protein fraction resulting from the initial conditions as P^{13} and the newly synthesized proteins, P^{12} . We can therefore set:

$$P_t = P_0 e^{\mu t} \quad (\text{Eq. 1})$$

with

$$P_t = P_t^{12} + P_t^{13} \quad (\text{Eq. 2})$$

We made the basic assumption that, as in most systems, protein degradation follows first order kinetics. Therefore,

$$P_t^{13} = P_0^{13} e^{-kt} \quad (\text{Eq. 3})$$

Because

$$P_0 = P_0^{13} \quad (\text{Eq. 4})$$

We obtained the following equality,

$$P_t^{12} = P_0 e^{\mu t} - P_0^{13} e^{-kt} \quad (\text{Eq. 5})$$

Combining Eq. 3 and 5

$$\frac{P_t^{12}}{P_t^{13}} = \frac{P_0 e^{\mu t} - P_0^{13} e^{-kt}}{P_0^{13} e^{-kt}} = \frac{e^{\mu t}}{e^{-kt}} - 1 \quad (\text{Eq. 6})$$

The natural log transformation of Eq. 6 allows us to set

$$\ln \left[\frac{P_t^{12}}{P_t^{13}} + 1 \right] = (\mu + k)t \quad (\text{Eq. 7})$$

with $\left[\frac{P_t^{12}}{P_t^{13}} \right] = r$

The half-life of the proteins was computed by extracting k from the experimental data as follows:

$$k = \frac{\sum_{i=1}^m \text{Ln}[r_i + 1] t_i}{\sum_{i=1}^m t_i^2} - \mu \quad (\text{Eq. 8})$$

with $T_{1/2} = \frac{\text{Ln}2}{k}$

$T_{1/2}$ for each protein was calculated for each technical replicate, excluding outliers, defined as those that differed by more than one standard deviation from the mean $T_{1/2}$.

Functional analyses—Lists of proteins identified in the different experimental conditions were analyzed using the GO Slim mapper tool, available at the Candida Genome Database website (<http://www.candidagenome.org/>). GO term enrichment analyses are provided with their corresponding p values computed using a hypergeometric distribution (Threshold 0.05).

RESULTS

^{12}C -based SLIM-labeling Increases Peptide and Protein Scores, the Number of Identifications, and Protein Sequence

Coverage—We performed bottom-up proteomic analyses on a simple eukaryotic unicellular organism, the pathogenic yeast, *C. albicans*, grown on a synthetic medium containing either U- ^{12}C -glucose or normal glucose as the sole carbon source. We investigated the effect of diluting ^{12}C with normal carbon in experiments in which protein samples from yeast under U- ^{12}C conditions were mixed with various amounts of protein from yeast under normal glucose conditions. Increasing the amount of ^{12}C in a peptide results in an exponential increase in the intensity of the monoisotopic ion. This intensity change depends on the total number of carbon atoms present in the peptide (supplemental Fig. S1). The resulting intense monoisotopic ion markedly improved bottom-up proteomics analyses. Increasing ^{12}C incorporation resulted in better overall scores (Fig. 1A) per identified peptide, with average scores up to 28.5% higher (Fig. 1B, 1C), leading to an average increase of the protein identification scores of 36% (Fig. 2B), with better sequence coverage (Fig. 2C). The number of identified peptides and proteins in *C. albicans* also increased by 14.1% and 11.3%, respectively, when applying a 1% FDR filter after ^{12}C enrichment *in vivo* (Fig. 1A, Fig. 2A and supplemental Table S1). Merging the different datasets produced in this study improved the known proteome coverage by 20% (23), with 5206 protein identifications from 57,322 identified peptide groups, without sample fractionation (supplementary File S1). Increases in peptide and protein scores and identifications did not correlate with lower isolation interferences for precursor ions. U- ^{12}C and natural carbon samples have similar global isolation interferences for MS precursors of 33.18% and 32.35%, respectively. The overall improvement in MS/MS interpretation and peptide and protein identification following ^{12}C enrichment is mostly because of the increase of monoisotopic ion abundance, resulting in more intense precursors and fragment ions and a global increase in the signal-to-noise ratio in MS/MS spectra (Fig. 1D). Globally, identification of peptides of all lengths was largely improved by the ^{12}C labeling method, except for peptides with neutral masses under 1000 Da (Fig. 3A) or eight amino acids (Fig. 3B), for which the number of identifications was similar to that under natural carbon condition. The number of peptide identifications was slightly lower under the U- ^{12}C condition than other ^{12}C containing conditions (Fig. 1A), but remained higher than under normal carbon condition.

A New Approach to Quantitative Proteomics Using ^{12}C -based SLIM-labeling—A key property of the isotopic cluster obtained under our experimental condition is that it contains both the required information for peptide identification, as well as accurate quantitation of peptide abundance changes, when samples are multiplexed. This quantitative aspect relies on the compositional variation of the isotopic cluster profile. We applied the ^{12}C labeling strategy to address one of the most challenging problems in modern biology, the analysis of the dynamics of proteome-wide variations in composition and structure, which is based on quantitative proteomics of a time

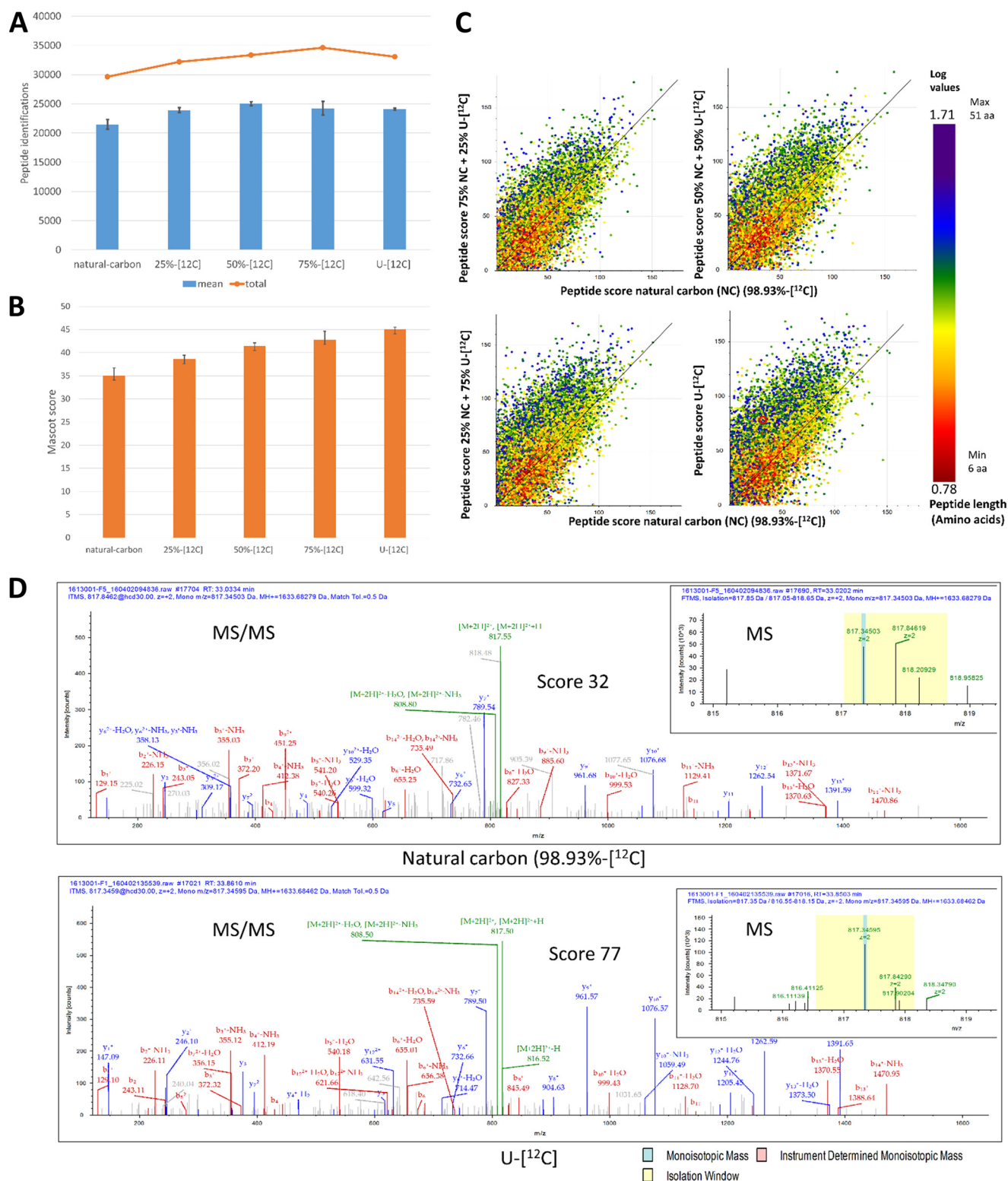


FIG. 1. Improvement of peptide identification and scoring by ^{12}C labeling. A, Number of peptides identified by LC-MS/MS, depending on ^{12}C enrichment (mean \pm S.D., $n = 3$ technical replicates). B, Histograms representing the mean peptide Mascot scores, depending on ^{12}C composition. C, Peptide scores for various ^{12}C compositions plotted against the scores of peptides under the control condition. The color code is based on peptide length. Each ^{12}C incorporation condition showed a similar total ion current in chromatograms (supplemental Fig. S2). D, Example (peptide in red circle in figure 1c) of the improvement in precursor isolation, MS/MS signal/noise, and Mascot scores using ^{12}C labeling (peptide QNEGEDGDGDELEVK).

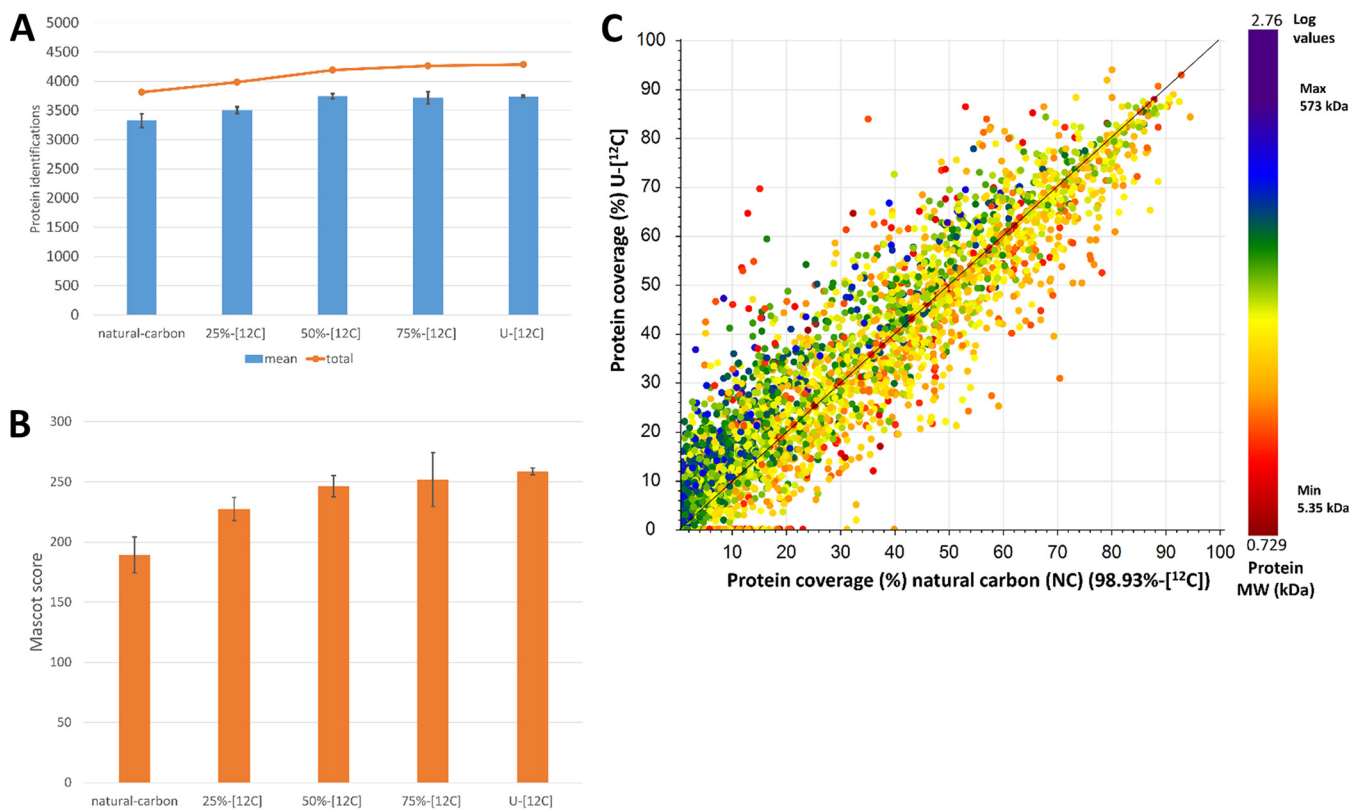


FIG. 2. Improvement of protein identification and scoring by ^{12}C labeling. A, Number of proteins identified by LC-MS/MS, depending on ^{12}C enrichment (mean \pm S.D., $n = 3$ technical replicates). B, Histograms representing the mean protein Mascot scores depending on ^{12}C composition. C, Protein sequence coverages for the U-[^{12}C] composition plotted against the protein sequence coverages under the control condition. The color code is based on protein length. Each ^{12}C incorporation condition showed a similar total ion current in chromatograms (supplemental Fig. S2).

series. Previous dynamic carbon labeling experiments in yeast have shown that the amino acid pool turns over in minutes (24). Shifting the cells from normal glucose to U- ^{12}C -glucose containing growth medium allowed us to produce uniformly ^{12}C -labeled amino acids. We used this property to measure *in vivo* protein turnover in time course experiments (15, 30, 60, 120, and 240 min). Normal turnover was perturbed by adding either MG132, an inhibitor of the proteasome protein-degradation machinery, or PMSF, a general serine-protease inhibitor which mostly targets vacuolar proteases in yeast, to the growth media (16). The ^{12}C -labeled proteins contained more of the light carbon isotope. One single isotope cluster per peptide contained all the necessary information for both identification and quantification, making this labeling strategy an interesting alternative to others (Fig. 4A).

We successfully analyzed the different data sets produced and evaluated the limits of application of the ^{12}C labeling method. When the level of ^{12}C incorporation was close to that in the U-[^{12}C] medium, we had some difficulties to measure peptide abundance using either Progenesis-LC for Proteomics, Progenesis-LC for metabolomics, or the precursor ion area node from Proteome Discoverer, despite higher identification levels under these conditions (Fig. 3C and Table I). Comparison of plots showing the total number of quantified

peptides in natural carbon (Fig. 3D) and peptides that were not quantified in U-[^{12}C] (Fig. 3E) showed that the concerned peptides were generally both low in abundance and short. However, the problem of abundance measurements became nearly negligible under the 75%-[^{12}C] condition (Fig. 3F) and was further reduced under the other ^{12}C conditions (data not shown).

Data Processing and Determination of Protein Half-lives—A key step in the analytical process is the determination of the abundance of ^{12}C from the isotope clusters for each peptide. The detailed data processing workflow is described in supplemental Fig. S3. It relies on the (i) accurate measurement of isotopolog abundance from which ^{12}C enrichment ratios (R_{iso}) are computed, (ii) identification of each peptide, and (iii) determination of the equation for ^{12}C incorporation in the peptide sequence for each peptide (supplementary File S2). This last step uses calibration curves generated by mixing protein extracts of known ^{12}C composition or by computing their theoretical values. We only considered peptides for which the difference between both values was less than 20% to minimize possible misidentification, despite a good correlation ($R^2 = 0.8335$) between the two data sets (supplemental Fig. S4A). Peptides satisfying this 20% cutoff represented 82.7% of the total peptides (25,990 and 5438 peptides below and

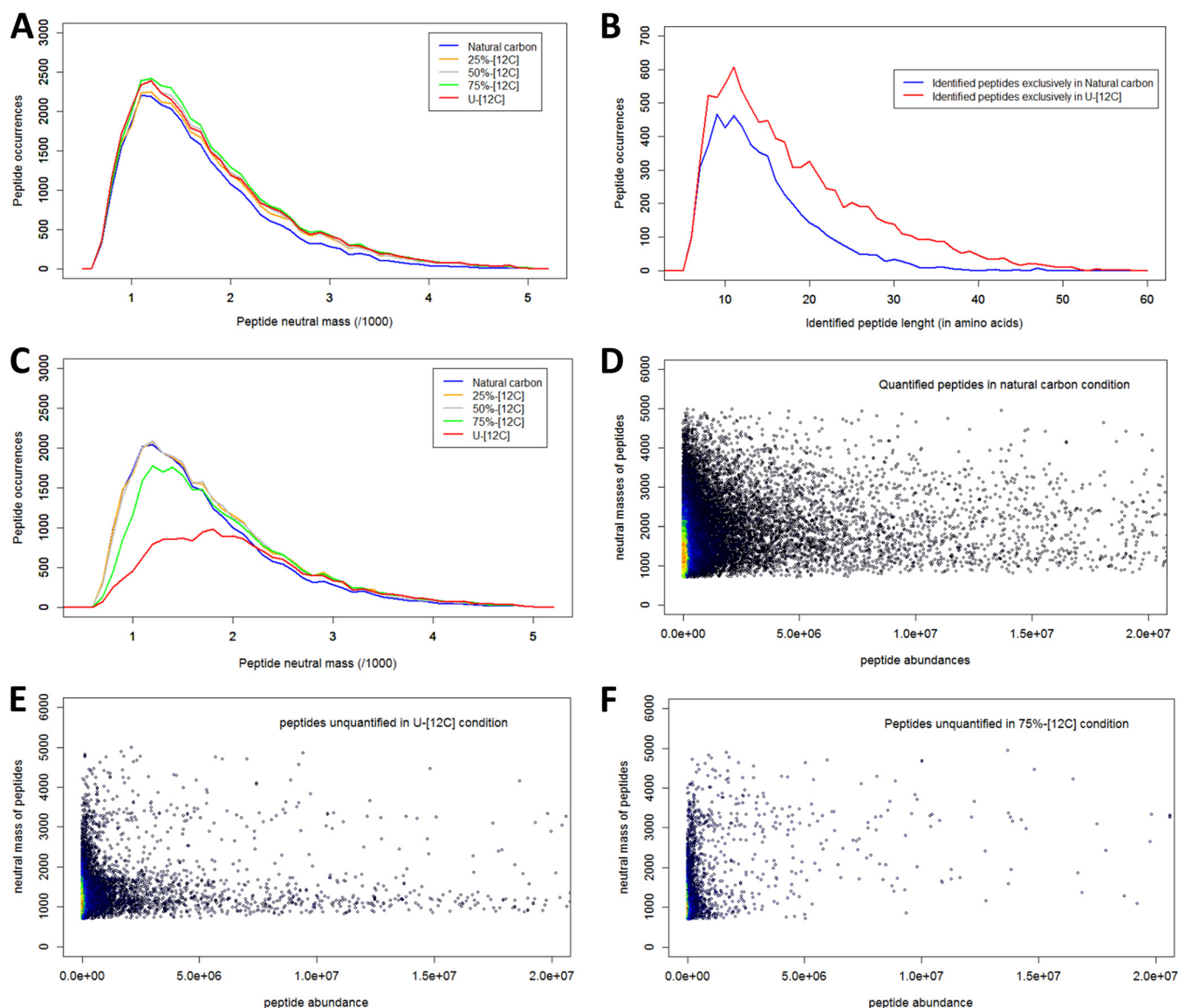


FIG. 3. Evaluation of the consequences of using the ^{12}C labeling method on peptide identification and abundance measurements. A, Occurrence of identified peptides by LC-MS/MS, depending on peptide neutral mass (/1000) and ^{12}C enrichment. B, Occurrence of peptides identified exclusively under the natural carbon or U-[^{12}C] conditions (with respect to each other), depending on peptide length (in amino acids). C, Occurrence of quantified peptides, depending on peptide neutral mass (/1000) and ^{12}C enrichment. D, Density plot of quantified peptides under the natural carbon condition, according to their neutral masses and measured abundances. Density plots of unquantified peptides in the U-[^{12}C] E, 75%-[^{12}C] F, conditions, according to their neutral masses and abundances measured under the natural carbon condition.

above the cutoff, respectively). The analysis of theoretical isotope clusters of peptides, such as those computed using MIDAs, showed that this strategy is superior to the more commonly used ^{13}C labeling, in which the incorporation of trace amounts of ^{12}C containing components results in broadening of the isotopic cluster and possible confusion in determining the actual monoisotopic ion (supplemental Fig. S5). We successfully used both calibration curves, showing that theoretical calibration curves can be used in the absence of experimental data. The general workflow for the determination of protein turnover is described in Fig. 4B. It relies on the (i) measurement of ^{12}C incorporation in peptides as a

function of time (Fig. 4A and [Supplementary File S3](#)); (ii) aggregation of individual peptide data for protein assembly (only peptides with incorporation rates equal to the mean \pm one S.D. are considered for further processing); and (iii) computation of protein turnover ($T_{1/2}$) based on the exponential model of protein synthesis and degradation (25). We only considered proteins that exhibited a linear relationship between $\ln(r+1)$ versus time, where r is the light/heavy protein ratio, with an R^2 greater than 0.9 for the protein turnover determination (Fig. 5B and [supplementary File S4](#)), if at least four time points were validated. This is a conservative approach for the determination of the $T_{1/2}$ that strengthens the

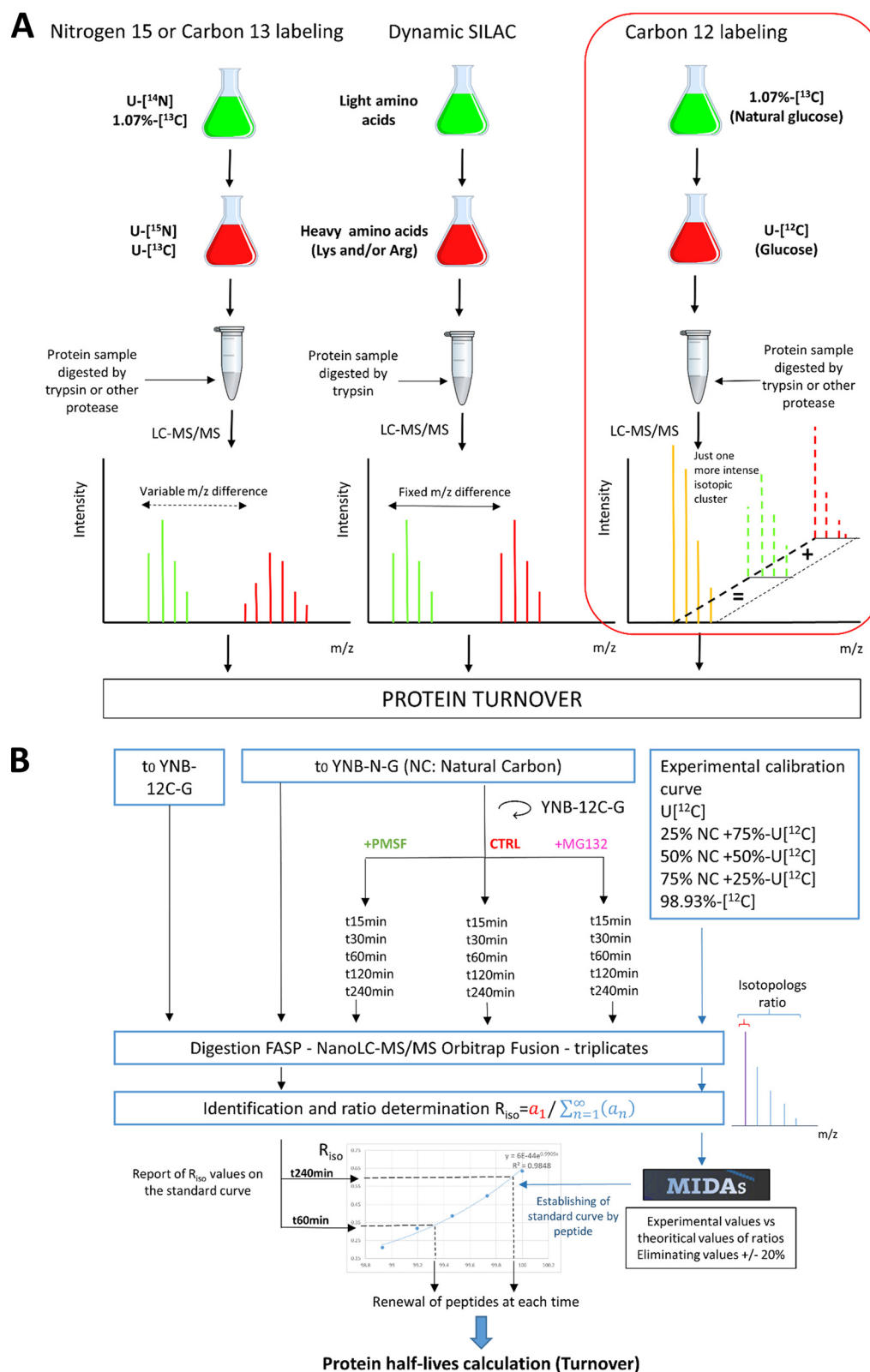


FIG. 4. Principle of the new metabolic labeling strategy using ¹²C-based SLIM-labeling. A, Comparison with other existing methods for determining proteome-wide protein turnover. The ¹²C labeling strategy allows direct evaluation of the contribution of labeled and unlabeled peptides within a single isotope cluster instead of the two observed in other metabolic labeling methods. B, General workflow used in this study for protein half-life determination. The details of the procedure are described in [supplemental Fig. S3](#).

TABLE I

Occurrences of identified and quantified peptides/proteins depending of the ^{12}C composition. As a remark, for peptide and protein identification, values are not exactly the same as those presented in the Figs. 1A, 2A and the supplementary Table I because each raw files from the different ^{12}C composition conditions were searched for identification here separately with Proteome Discoverer 2.1

	Natural carbon	25%-[^{12}C]	50%-[^{12}C]	75%-[^{12}C]	U-[^{12}C]
Identified peptides	28460	31193	32639	33723	32624
Quantified peptides	26615	28670	28410	25481	17085
% peptides Quantified/identified	93.51	91.91	87.04	76.63	52.37
Identified proteins	3377	3568	3768	3786	3816
Quantified proteins	3253	3382	3494	3364	3126
% proteins Quantified/identified	96.33	94.79	92.73	88.85	81.92

confidence between replicates (S.D. < 14.4%) relative to using less stringent parameters (supplemental Table S2). ^{12}C incorporation and protein turnover measurements were robust and the variability between replicates was low (supplemental Fig. S4B and supplemental Fig. S6A). We obtained very similar results for the turnover determination, whether we computed the ^{12}C incorporation into peptides using the experimental or theoretical calibration curves (supplemental Fig. S6B).

Impact of Inhibiting Proteasome Or Vacuolar Degradation Systems On Protein Half-life and Abundance—We shifted growing cells from a normal glucose containing medium to a U-[^{12}C] glucose containing medium. This allowed us to experimentally measure the rate of ^{12}C amino acid incorporation into newly synthesized proteins. Measuring the variation of isotopolog abundance for each peptide over time allowed us to compute the half-lives of proteins at the proteome scale. We determined the half-life of 2346, 2406, and 2263 proteins under the control, MG132, and PMSF conditions, respectively (supplementary File S5). Some proteins, such as CaSit4p, were rapidly replaced by newly synthesized copies of high ^{12}C content, whereas others, such as CaSod3p, appeared to be extremely stable with low ^{12}C incorporation (Fig. 5C). The mean half-life in our datasets were 2.58, 2.64, and 4.0 h for the control, MG132, and PMSF conditions, respectively (Fig. 5D, supplemental Table S2). The median half-lives were 2.42, 2.13, and 3.08 h for the control, MG132, and PMSF conditions, respectively (Fig. 5D, supplemental Table S2). Median values of protein half-life for the control and MG132 conditions were different, whereas their mean values were quite similar. Both median and mean values increased under the PMSF condition. These results show that the half-life of proteins with short half-lives increased under the MG132 condition, whereas those with long half-lives increased under the PMSF treatment (Fig. 5D).

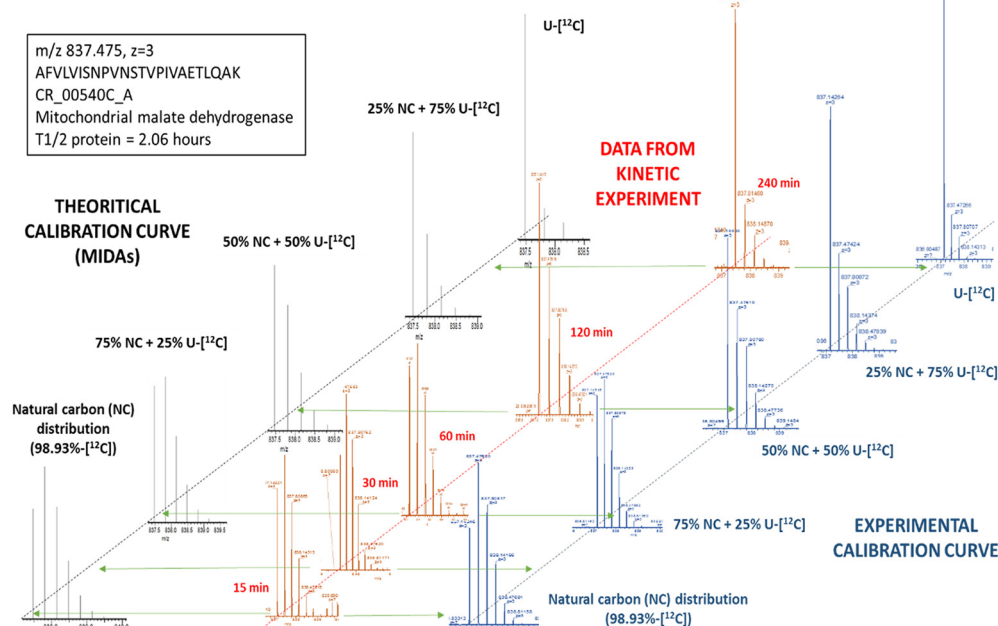
Functional analysis by enrichment of gene ontology terms show that, under the control condition, proteins involved in translation, ribosomal proteins (essentially the RPL, RPS, and RPP ribosomal proteins), and proteins from the extracellular region and the cell wall had long half-lives, whereas cell cycle proteins or those of the endomembrane system had mostly short half-lives (supplemental Table S3).

We combined the analyses of the variation in protein turnover to label-free quantification of their abundance to gain more insights into the dynamics of protein turnover under the three conditions analyzed by defining clusters of proteins with similar changes in turnover and abundance among the control, MG132-treated, and PMSF-treated datasets (Fig. 6, supplementary File S6). One of the most significant cluster (cluster H) contains most proteins involved in proteasome structure and function (GO terms protein catabolic process and peptidase activity, p value = $3.19\text{e-}15$ and $2.65\text{e-}11$, respectively). In this cluster, MG132 treatment led to a marked decrease in the half-life of the structural α -subunit (Pre5p, Pre6p, Pre8p, Pre9p, Pre10p, Pup2p), catalytic β -subunit (Pre2p, Pre3p, Pup1p), proteasome-interacting proteins (Rpn1p, Rad6p, Rad23p), and associated ATPases (Cdc48p, Rpt1p, Rpt6p) (Fig. 6, supplementary Fig. 7). The abundance of proteasome constituents measured by label-free quantitative proteomics increased at every time point under the MG132 condition (Fig. 6, Fig. 7A). This indicates the synthesis of these constituents in response to the inhibition of the proteasome. There were no global changes in abundance for these proteins under the PMSF condition during the time course experiment (Fig. 7B), whereas their half-life significantly increased. Altogether, these results suggest the inhibition of proteasome component degradation under PMSF treatment.

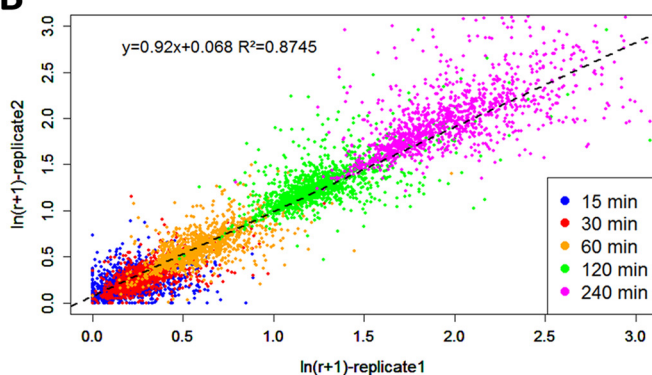
The proteins from cluster B (Fig. 6) showed large increases in protein half-life and abundance under the PMSF condition, whereas these parameters decreased slightly under the MG132 condition. Gene ontology terms analysis showed that these proteins are involved in translation (p value = $2.54\text{e-}7$) and ribosome structure (p value = $1.4\text{e-}4$). The variations of $T_{1/2}$ and abundance in this group suggest that these corresponding proteins were particularly targeted by the vacuolar degradation system under the control condition.

We obtained a third characteristic profile (Fig. 6, cluster E) in which the protein half-life increased and the corresponding protein abundance (supplementary File S6) decreased under the PMSF condition, whereas there was no variation under the MG132 condition. This suggests that the synthesis of these proteins was inhibited in response to PMSF treatment. The GO terms enrichment statistics were weaker and pointed

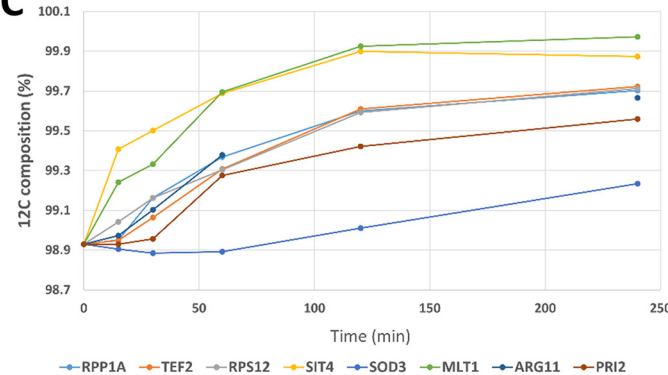
A



B



C



D

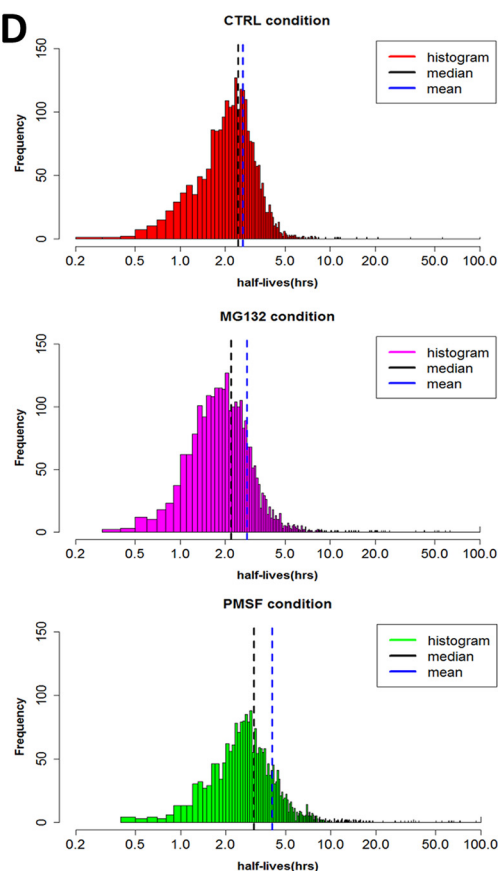


FIG. 5. Determination of protein half-lives and robustness of the method. A, Example of a peptide half-life determination by comparing the isotopic distribution of the peptide AFVLVISNPVNSTVPIVAETLQAK for each time point with distributions obtained using experimental and theoretical calibration curves. B, Plots of $\ln(r+1)$ values with r representing the light/heavy protein ratio for replicates 1 and 2 at each time point. C, Examples of the kinetics of ¹²C incorporation for specific proteins. D, Density plot of $T_{1/2}$ values under the control, MG132, and PMSF conditions. Additional plots describing the robustness of $T_{1/2}$ measurements are shown in [supplemental Fig. S6](#).

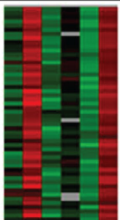


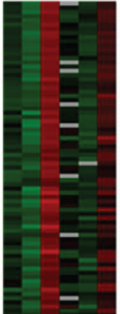


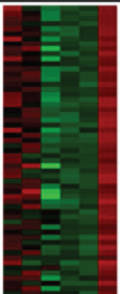


Clusters	Gene ontology analysis, % cluster (% total), p-value	Protein examples	Interpretations		
			Abundance (MG132, PMSF)	T _{1/2} (MG132, PMSF)	Comments
 H	<ul style="list-style-type: none"> - Protein catabolic process, 42.3 (6.1), 3.19e-15 - Peptidase activity, 28.8 (3.7), 2.65e-11 - Endoplasmic reticulum, 17.3 (6.8), 0.0045 - Response to stress, 28.8 (14.8), 0.0037 - Idem for clusters F,I 	CDC48, DDI1, GGA2, PRE10, PRE2, PRE3, PRE5, PRE6, PRE8, PRE9, PUP2, PUP3, RAD23, RAD6, RPN1, RPT1, RPT6, SCL1			<ul style="list-style-type: none"> - Synthesis of proteasome components in response to MG132 - Inhibition of the degradation of proteasome components in response to PMSF
 B	<ul style="list-style-type: none"> - Translation, 26.3 (7.9), 2.54e-07 - Ribosome biogenesis, 15.8 (8.7), 0.015 - Ribosome, 21.1 (8.2), 0.00014 - Idem for clusters A, C, J 	GIR2, HCR1, MRP2, MRP7, MRPL8, MRPS9, NPL3, RPL10A, TIF11, TIF5			The translation machinery is specifically targeted by the vacuolar degradation system
 E	<ul style="list-style-type: none"> - Peroxisome, 10.2 (3.1), 0.0061 - Plasma membrane, 16.9 (9.4), 0.025 - Carbohydrate metabolic process, 15.8 (5.8), 0.0031 - Idem for cluster D 	FAA4, GLK1, OSH3, PNG2, RDI1, SEC4, SLK19, AAT21, ACH1, CAT2, CIT1, CYP1, ECI1, GCY1, GLK1, HSP104			Inhibition of synthesis associated to the PMSF treatment

FIG. 6. Classification of proteins based on their T_{1/2} and difference in abundance under the different experimental conditions (control, MG132, and PMSF treatment). Description of several clusters (determined by the Autoclass Bayesian clustering system) using the calculated protein T_{1/2} values and corresponding protein abundances determined by quantitative label-free analysis (240 min time point) under control, MG132, and PMSF conditions. All clusters are described in [supplementary file S6](#). We obtained similar results when the data were processed using either the experimental (with three time points or more) or theoretical calibration curves.

toward proteins localized mainly in peroxisomes or the plasma membrane ([supplemental Table S4](#)).

PMSF is a general inhibitor of serine proteases. We thus measured the changes in abundance of the serine proteases annotated in the Candida Genome Database. There were no global changes in the abundance of these proteases under the MG132 condition (Fig. 7C, [supplementary File S7](#)). There was a transient increase in the abundance of some serine proteases (Cpy1p, Imp1p, Kex1p, Prc2p, Ssy5p) after 15 min under the PMSF condition (Fig. 7D), followed by a return to similar levels as under the control condition. We did not observe similar changes in the abundance of annotated amino-peptidases, which did not change, either under the MG132 or PMSF conditions (Fig. S7E, S7F).

DISCUSSION

The proposed SLIM-labeling strategy allows direct evaluation of the contribution of labeled and unlabeled peptides within a single isotope cluster instead of the two observed in other metabolic labeling methods. This is a major advantage over methods in which the mass shift between labeled and unlabeled peptides is variable and depends on the total number of labeled atoms. It avoids the problem of peptide matching encountered in methods dependent on sample multiplexing, while also making more time available for mass spectrometer data acquisition. The amount of each precursor for MS/MS analyses is increased by at least 2-fold and the higher intensity of the monoisotopic ion provides a signifi-

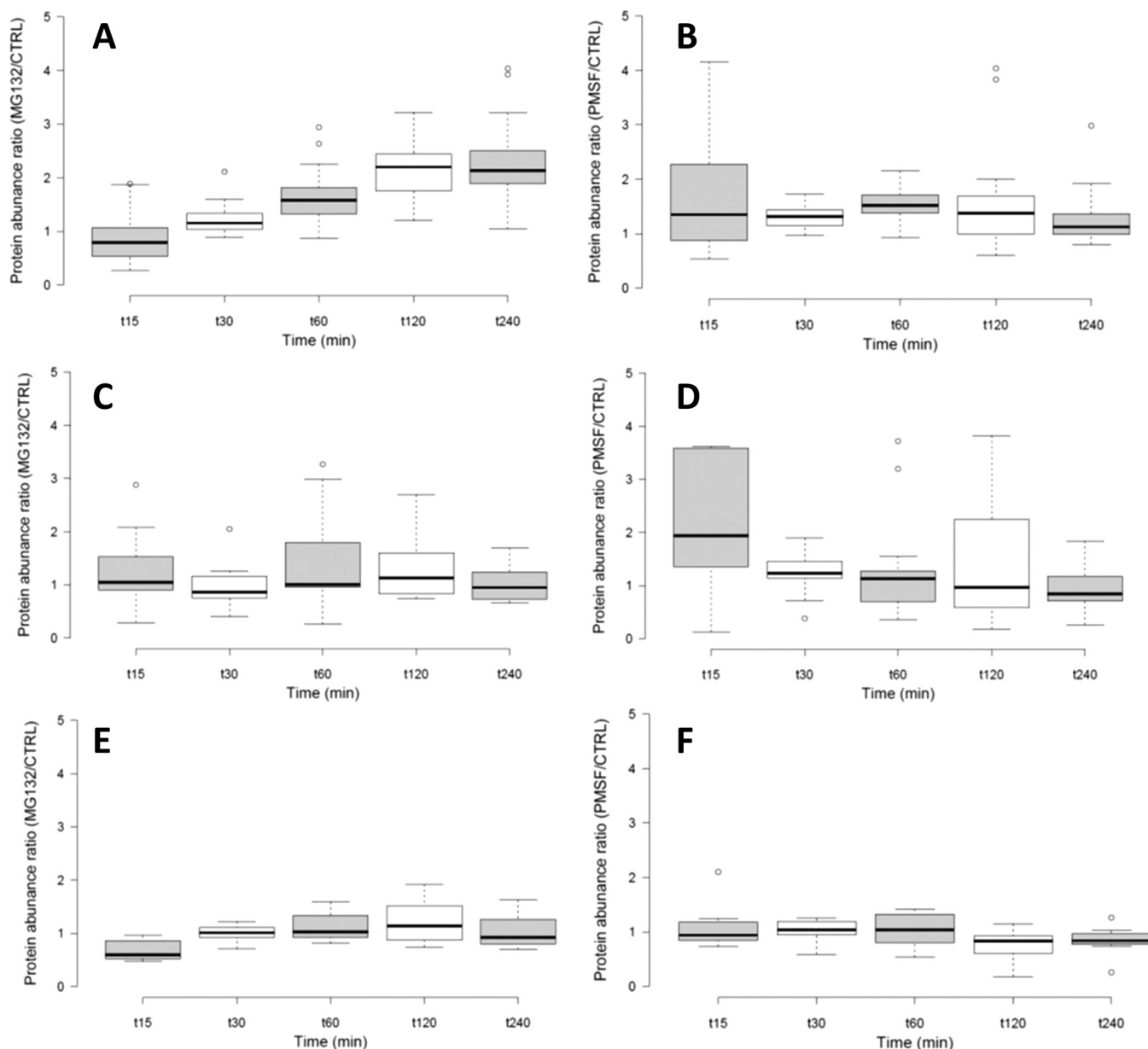


FIG. 7. Boxplot of the changes over time in the abundance of proteasome components and peptidases under the different experimental conditions (control, MG132, and PMSF treatment). Protein abundance ratios of MG132 *versus* Control are represented in a, c, and e and PMSF *versus* Control in b, d, and f. Abundance ratios of proteasome constituents (proteases and regulators) (A, B), characterized serine proteases (C, D), and amino-peptidases (E, F) are represented. Proteasome components (A, B): C2_07220W_A, C6_00760W_A, CR_09580C_A, HSM3, NAS6, PRE1, PRE10, PRE2, PRE3, PRE4, PRE5, PRE6, PRE7, PRE8, PRE9, PUP1, PUP2, PUP3, RPN10, RPN11, RPN12, RPN2, RPN3, RPN6, RPN7, RPN8, RPN9, RPN9, RPT1, RPT2, RPT4, RPT5, RPT6, SLC1, UBP6, UMP1. Characterized serine proteases (C, D): C6_01470W_A, CPY1, DAP2, IMP1, IMP2, KEX1, KEX2, NMA111, PRB1, PRB12, PRC2, PRC3, SEC11, SSY5. Characterized amino-peptidases (E, F): APE3, C1_10820C_A, C1_14450C_A, C3_03560W_A, DAP2, LAP3, LAP4, LAP41.

cantly improved signal-to-noise ratio. These specific features make the overall identification process more efficient than in other metabolic labeling methods. We also avoid the problem of amino acid conversion, because all amino acids contain ^{12}C . Therefore, the chemistry of peptide production is not restricted to trypsin, a problem frequently encountered with SILAC labeling. Here, we used $\text{U-}^{12}\text{C}$ -glucose as the sole

carbon source in a prototrophic yeast strain. Thus, all ^{12}C amino acids resulted from glucose catabolism. By considering all the datasets, we identified 5206 proteins for 57,322 peptides in *Candida albicans* without a sample fractionation step. This enriches the coverage of the *C. albicans* proteome publicly available by 25%, which was composed of 4174 canonical proteins for 6218 proteins in the predicted proteome (26).

We established the optimal conditions of the ^{12}C -based SLIM-labeling method by analyzing peptide and protein identification and quantification using (i) both experimental calibration curves and their theoretical counterparts and, (ii) *in vivo* labeling experiments in which cells grown under normal glucose condition were shifted to a U- ^{12}C -glucose medium making it possible to follow ^{12}C incorporation into proteins over time (turnover determination experiments). We prepared sample sets by mixing known amounts of U- ^{12}C labeled peptides with increasing amounts of peptides prepared from yeast grown under the control conditions (normal carbon composition). More peptides were identified for cells grown under all ^{12}C conditions than those grown under the control condition. However, there was a slight decrease in the number of peptide identifications in the U- ^{12}C condition. This decrease can be because, although ^{12}C labeling increased the identification rates of all classes of peptides, there are difficulties in determining the charge state of the smaller peptides with low intensity for which the only detectable ion was the monoisotopic mass. This problem had only a limited impact on the global proteomics analysis, because peptides with a small number of amino acids are often non-informative, because they often belong to several proteins and are therefore not unique. However, we obtained more peptide and protein identifications under all ^{12}C conditions than the “normal carbon” condition.

One key feature of the SLIM-labeling technique is the possibility to extract quantitative data from a single isotope cluster by measuring the ratio between the monoisotopic ion and all detected isotopologs. The principal limitation of our method was that the software used for quantitative proteomics (Progenesis Q1 for Proteomics, Progenesis Q1 for Metabolomics, Proteome Discoverer) to determine isotopolog abundances did not allow us to measure the abundance of small peptides of low abundance when their ^{12}C composition was close to that of the U- ^{12}C condition. The abundance detection limits can be improved with appropriate editing of the peptide property definitions, currently based on the classical averagine model, and is under evaluation. Most peptides were not completely labeled with ^{12}C for each time point after shifting from normal glucose to U- ^{12}C -glucose during the turnover experiments. The abundance measurement problem concerned only a limited number of peptides. Furthermore, we considered only peptides with at least three or four ^{12}C incorporation values of the five calibration points to establish the experimental calibration curve. Thus, if the abundance of a given peptide was not measured under the U- ^{12}C condition, the determination of the experimental calibration curve of this peptide remained possible.

We demonstrated the power of isotope complexity reduction *in vivo*, using ^{12}C -based SLIM-labeling in pulsed mode. This allowed, for the first time, the determination of protein turnover at the proteome scale in *C. albicans*. We determined the half-life of 2346 proteins under the control

condition, and 2406 and 2263 proteins under the MG132 and PMSF conditions, respectively. We used stringent filters to validate our results. Our model for protein half-life measurements also considered the degradation rate of proteins, a parameter not always taken into account (e.g. (27)). We found a mean protein half-life of 2.58 h (median = 2.42). Martin-Perez *et al.* (27) compiled the median half-lives for *Saccharomyces cerevisiae* proteins for several studies. They exhibited a wide range of values from 43 min (28), to 1.8 h (27), 8.8 h (26), 10.8 h (29), and even 34 h (30). Such discrepancies highlight the presence of methodological problems. Some are likely related to not accounting for either individual protein degradation rates (k) (27) or the growth rate of the cells from which the proteomes were analyzed. Here, we applied the simple formalism described by Schwanhaussner *et al.* (22), which considers both factors and in which proteins from the initial conditions may be considered to have incorporated “heavy” amino acids, whereas the newly synthesized proteins incorporated only “light” amino acids, providing a simple model for half-life measurements. This approach makes a clear difference between protein turnover ($T_{1/2} = \ln 2/k$) and the parameter $t_{1/2}$, the time required to reach a protein-(heavy)/protein(light) ratio of 1/2. When k trends to 0, $T_{1/2}$ trends to infinity, but $t_{1/2}$ is close to the doubling time of the cells. Our experimental data fitted well with the exponential model (more than 88% of $\ln(r+1)$ values fitted with $R^2 > 0.9$). However, 12% of the measurements exhibited more complex ^{12}C incorporation patterns, with a few fitting a sigmoid model, corresponding to a logistic function, as described by Martin-Perez *et al.* (27). The lack of an explicit formulation of this function prevented us from computing accurate half-lives for these proteins. In this context, a recent study by McShane *et al.* (31) that analyzed the kinetics of protein stability showed that a significant number of cellular proteins were characterized by a non-exponential degradation (NED) process, which, according to the authors, was related to protein aging and folding, with the newly synthesized proteins being more prone to NED. NED was furthermore attributed, in part, to proteasome activity (31).

The functional analysis of protein turnover by enrichment in gene ontology terms showed that proteins involved in translation and ribosomal proteins (essentially RPL, RPS, and RPP ribosomal proteins) had long half-lives, as described for *S. cerevisiae* and *Sch. pombe* (26), whereas cell cycle proteins were mostly represented in categories with short half-lives, as described in budding yeast (28). The definition of “short” or “long” half-lives was completely dependent on the definition of the mean half-lives in the proteomes studied and is a source of discrepancy between published data sets.

We evaluated the effects of a vacuolar degradation inhibitor (PMSF) and a proteasome inhibitor (MG132) on protein half-lives. The half-lives of many more proteins were affected by PMSF treatment than that with MG132. This may be related to the fact that PMSF mainly targets serine proteases of the

vacuolar protein degradation system, described as a generalist degradation pathway, by globally targeting most proteins, including, several specific classes of proteins, such as ribosome biogenesis components. The proteasome represents a more specific degradation pathway. The proteasome is involved in the degradation of newly synthesized protein components of macromolecular complexes and, more generally, short-lived proteins, whereas long-lived proteins are mainly degraded by the vacuolar proteases (16, 32, 33). Our results are consistent with these assumptions, as we measured an increase in the occurrence of short-lived proteins in *C. albicans* cells treated with MG132, suggesting stabilization of these putative proteasome targets. Similarly, we observed that proteins with long half-lives accumulated in PMSF-treated cells.

Clustering proteins according to the similarities between $T_{1/2}$ and abundance in the different experimental conditions allowed us to characterize other specific variation profiles. The major effect of MG132 treatment was a decrease in the half-lives of proteasome constituents and an increase in their abundance, as shown in our quantitative label-free analysis. The increased rate of ^{12}C incorporation in proteasomal components, together with their increased abundance, indicates adaptive biosynthesis in response to inhibition of the proteasome and appears to correlate with an increase in the level of Hsm3p, a key regulator of proteasome assembly (34). It was previously shown that some components of the proteasome complex became more abundant in response to MG132 at the mRNA level for human cells (35) and at the protein level for *S. cerevisiae* cells (36). Our results compare favorably with the findings of Yu *et al.* (33), who demonstrated that human cells responded to the strong proteasome inhibitor BTZ by blocking the degradation of proteasome subunits and stabilizing the proteasome assembly factor PSMD10, which would further facilitate the assembly of proteasome subunits, leading to an increase in their abundance. These biological similarities can be a validation of the turnover measurements obtained by our quantitative ^{12}C -based SLIM-labeling strategy. The half-lives and abundance of the proteasome components changed differently when cells were exposed to PMSF. Their abundance remained constant, but their half-lives increased, suggesting the inhibition of a PMSF-dependent degradation pathway, leading to compensatory inhibition of proteasome component synthesis.

A large group of proteins involved in translation and ribosome function were very sensitive to the action of PMSF, with a large increase in both $T_{1/2}$ and abundance, suggesting the inhibition of their degradation, an effect that may be reinforced by the possible inhibition of their synthesis within the time scale of the experiment. PMSF treatment specifically induced a marked increase in the half-lives of cell-wall and membrane proteins, together with a decrease in their abundance, suggesting inhibition of their synthesis. The mechanism of PMSF-dependent signaling on the synthesis of specific classes of proteins is yet to be determined. We analyzed

the changes in abundance of various classes of characterized intracellular proteases in *Candida albicans*. No major changes could be attributed to either treatment, except for the specific effect of MG132 on proteasome proteases, excluding the possibility of defining an alternative pathway for protein degradation under PMSF or MG132-induced stress.

We show here that reducing the isotope complexity of proteins *in vivo* by the SLIM-labeling strategy provides a new way to access high performance, high-resolution, and high accuracy MS-based proteomics with significantly improved protein identification and efficient quantitative assessment of proteome variations. The general principle of this method can be extended to many organisms using appropriate carbon sources as metabolic precursors of amino acids *in vivo*. Our strategy proved to be very efficient even when the overall ^{12}C incorporation rate was low. This would allow the application of this approach to mammalian cell cultures, even though they require essential amino acids (not yet available as ^{12}C amino acids), as the expected amount of light labeling from glucose may be as high as 30–40% of the protein mass (37, 38). We are currently validating this method in multicellular organisms.

Acknowledgments—We thank Dr. Joel Louette, Cambridge Isotopes Laboratories, for initial discussions on the availability of U- ^{12}C] glucose, Dr. Gelio Alves, MQPB, NCBI, NIH for his help in setting the MIDAs standalone application, to the Region Ile-de-France (SESAME), the Paris-Diderot University (ARS), and CNRS for funding part of the LC-MS/MS equipment. The English text was edited by Alex Edelman & Associates.

DATA AVAILABILITY

The complete data sets are available in the PRIDE partner repository (39) under the identification number: PXD005364 as .raw files, Proteome Discoverer 2.1 .pdResult file, associated pep.xml and xlsx files, label-free report generated by Progenesis Q1, and the *C. albicans* protein sequence database, provided in fasta format.

* This work was funded in part by Region Ile-de-France (SESAME), the Paris-Diderot University (ARS), and CNRS.

§ This article contains [supplemental material](#). None of the authors declare competing financial interests.

¶ To whom correspondence should be addressed: Proteomics@IJM, Institut Jacques Monod, 15 Rue Helene Brion, Paris 75013 France. Tel.: 33-01-57278029; E-mail: jean-michel.camadro@ijm.fr.

REFERENCES

- Kim, T. Y., Wang, D., Kim, A. K., Lau, E., Lin, A. J., Liem, D. A., Zhang, J., Zong, N. C., Lam, M. P., and Ping, P. (2012) Metabolic labeling reveals proteome dynamics of mouse mitochondria. *Mol. Cell. Proteomics* **11**, 1586–1594
- Li, L., Nelson, C. J., Solheim, C., Whelan, J., and Millar, A. H. (2012) Determining degradation and synthesis rates of arabidopsis proteins using the kinetics of progressive ^{15}N labeling of two-dimensional gel-separated protein spots. *Mol. Cell. Proteomics* **11**, M111.010025
- Cargile, B. J., Bundy, J. L., Grunden, A. M., and Stephenson, J. L., Jr. (2004) Synthesis/degradation ratio mass spectrometry for measuring relative dynamic protein turnover. *Anal. Chem.* **76**, 86–97
- Ong, S. E., Blagoev, B., Kratchmarova, I., Kristensen, D. B., Steen, H., Pandey, A., and Mann, M. (2002) Stable isotope labeling by amino acids

- in cell culture, SILAC, as a simple and accurate approach to expression proteomics. *Mol. Cell. Proteomics* **1**, 376–386
5. Schwanhaussner, B., Gossen, M., Dittmar, G., and Selbach, M. (2009) Global analysis of cellular protein translation by pulsed SILAC. *Proteomics* **9**, 205–209
 6. Doherty, M. K., Hammond, D. E., Clague, M. J., Gaskell, S. J., and Beynon, R. J. (2009) Turnover of the human proteome: determination of protein intracellular stability by dynamic SILAC. *J. Proteome Res.* **8**, 104–112
 7. Shenoy, A., and Geiger, T. (2015) Super-SILAC: current trends and future perspectives. *Expert Rev. Proteomics* **12**, 13–19
 8. Scholten, A., Mohammed, S., Low, T. Y., Zanivan, S., van Veen, T. A., Delanghe, B., and Heck, A. J. (2011) In-depth quantitative cardiac proteomics combining electron transfer dissociation and the metalloendopeptidase Lys-N with the SILAC mouse. *Mol. Cell. Proteomics* **10**, O111.008474
 9. Tebbe, A., Klammer, M., Sighart, S., Schaab, C., and Daub, H. (2015) Systematic evaluation of label-free and super-SILAC quantification for proteome expression analysis. *Rapid Commun. Mass Spectrom.* **29**, 795–801
 10. Thorsell, A., Portelius, E., Blennow, K., and Westman-Brinkmalm, A. (2007) Evaluation of sample fractionation using micro-scale liquid-phase isoelectric focusing on mass spectrometric identification and quantitation of proteins in a SILAC experiment. *Rapid Commun. Mass Spectrom.* **21**, 771–778
 11. Marshall, A. G., Senko, M. W., Li, W., Li, M., Dillon, S., Guan, S., and Logan, T. M. (1997) Protein molecular mass to 1 Da by ¹³C, ¹⁵N double-depletion and FT-ICR mass spectrometry. *J. Am. Chem. Soc.* **119**, 433–434
 12. Rodgers, R. P., Blumer, E. N., Hendrickson, C. L., and Marshall, A. G. (2000) Stable isotope incorporation triples the upper mass limit for determination of elemental composition by accurate mass measurement. *J. Am. Soc. Mass Spectrom.* **11**, 835–840
 13. Shi, S. D., Hendrickson, C. L., and Marshall, A. G. (1998) Counting individual sulfur atoms in a protein by ultrahigh-resolution Fourier transform ion cyclotron resonance mass spectrometry: experimental resolution of isotopic fine structure in proteins. *Proc. Natl. Acad. Sci. U.S.A.* **95**, 11532–11537
 14. Compton, P. D., Zamborg, L., Thomas, P. M., and Kelleher, N. L. (2011) On the scalability and requirements of whole protein mass spectrometry. *Anal. Chem.* **83**, 6868–6874
 15. Kisselev, A. F., and Goldberg, A. L. (2001) Proteasome inhibitors: from research tools to drug candidates. *Chem. Biol.* **8**, 739–758
 16. Lee, D. H., and Goldberg, A. L. (1996) Selective inhibitors of the proteasome-dependent and vacuolar pathways of protein degradation in *Saccharomyces cerevisiae*. *J. Biol. Chem.* **271**, 27280–27284
 17. Alves, G., Ogurtsov, A. Y., and Yu, Y. K. (2014) Molecular Isotopic Distribution Analysis (MIDAs) with adjustable mass accuracy. *J. Am. Soc. Mass Spectrom.* **25**, 57–70
 18. Wilson, R. B., Davis, D., and Mitchell, A. P. (1999) Rapid hypothesis testing with *Candida albicans* through gene disruption with short homology regions. *J. Bacteriol.* **181**, 1868–1874
 19. Inglis, D. O., Arnaud, M. B., Binkley, J., Shah, P., Skrzypek, M. S., Wymore, F., Binkley, G., Miyasato, S. R., Simison, M., and Sherlock, G. (2012) The *Candida* genome database incorporates multiple *Candida* species: multispecies search and analysis tools with curated gene and protein information for *Candida albicans* and *Candida glabrata*. *Nucleic Acids Res.* **40**, D667–D674
 20. Achcar, F., Camadro, J. M., and Mestivier, D. (2009) AutoClass@IJM: a powerful tool for Bayesian classification of heterogeneous data in biology. *Nucleic Acids Res.* **37**, W63–W67
 21. Valkenborg, D., Mertens, I., Lemiére, F., Witters, E., and Burzykowski, T. (2012) The isotopic distribution conundrum. *Mass Spectrom. Rev.* **31**, 96–109
 22. Schwanhaussner, B., Busse, D., Li, N., Dittmar, G., Schuchhardt, J., Wolf, J., Chen, W., and Selbach, M. (2011) Global quantification of mammalian gene expression control. *Nature* **473**, 337–342
 23. Vialas, V., Sun, Z., Reales-Calderon, J. A., Hernaez, M. L., Casas, V., Carrascal, M., Abian, J., Monteoliva, L., Deutsch, E. W., Moritz, R. L., and Gil, C. (2016) A comprehensive *Candida albicans* PeptideAtlas build enables deep proteome coverage. *J. Proteomics* **131**, 122–130
 24. Hong, K. K., Hou, J., Shoaie, S., Nielsen, J., and Bordel, S. (2012) Dynamic ¹³C-labeling experiments prove important differences in protein turnover rate between two *Saccharomyces cerevisiae* strains. *FEMS Yeast Res.* **12**, 741–747
 25. Larrabee, K. L., Phillips, J. O., Williams, G. J., and Larrabee, A. R. (1980) The relative rates of protein synthesis and degradation in a growing culture of *Escherichia coli*. *J. Biol. Chem.* **255**, 4125–4130
 26. Christiano, R., Nagaraj, N., Frohlich, F., and Walther, T. C. (2014) Global proteome turnover analyses of the Yeasts *S. cerevisiae* and *S. pombe*. *Cell Reports* **9**, 1959–1965
 27. Martin-Perez, M., and Villen, J. (2015) Feasibility of protein turnover studies in prototrophic *Saccharomyces cerevisiae* strains. *Anal. Chem.* **87**, 4008–4014
 28. Belle, A., Tanay, A., Bitincka, L., Shamir, R., and O'Shea, E. K. (2006) Quantification of protein half-lives in the budding yeast proteome. *Proc. Natl. Acad. Sci. U.S.A.* **103**, 13004–13009
 29. Helbig, A. O., Daran-Lapujade, P., van Maris, A. J., de Hulster, E. A., de Ridder, D., Pronk, J. T., Heck, A. J., and Slijper, M. (2011) The diversity of protein turnover and abundance under nitrogen-limited steady-state conditions in *Saccharomyces cerevisiae*. *Mol. bioSystems* **7**, 3316–3326
 30. Pratt, J. M., Petty, J., Riba-Garcia, I., Robertson, D. H., Gaskell, S. J., Oliver, S. G., and Beynon, R. J. (2002) Dynamics of protein turnover, a missing dimension in proteomics. *Mol. Cell. Proteomics* **1**, 579–591
 31. McShane, E., Sin, C., Zauber, H., Wells, J. N., Donnelly, N., Wang, X., Hou, J., Chen, W., Storchova, Z., Marsh, J. A., Valleriani, A., and Selbach, M. (2016) Kinetic Analysis of Protein Stability Reveals Age-Dependent Degradation. *Cell* **167**, 803–815 e821
 32. van der Lee, R., Lang, B., Kruse, K., Gsponer, J., Sanchez de Groot, N., Huynen, M. A., Matouschek, A., Fuxreiter, M., and Babu, M. M. (2014) Intrinsically disordered segments affect protein half-life in the cell and during evolution. *Cell Reports* **8**, 1832–1844
 33. Yu, T., Tao, Y., Yang, M., Chen, P., Gao, X., Zhang, Y., Zhang, T., Chen, Z., Hou, J., Zhang, Y., Ruan, K., Wang, H., and Hu, R. (2014) Profiling human protein degradome delineates cellular responses to proteasomal inhibition and reveals a feedback mechanism in regulating proteasome homeostasis. *Cell Res.* **24**, 1214–1230
 34. Barrault, M. B., Richet, N., Godard, C., Murciano, B., Le Tallec, B., Rousseau, E., Legrand, P., Charbonnier, J. B., Le Du, M. H., Guerois, R., Ochsenbein, F., and Peyroche, A. (2012) Dual functions of the Hsm3 protein in chaperoning and scaffolding regulatory particle subunits during the proteasome assembly. *Proc. Natl. Acad. Sci. U.S.A.* **109**, E1001–E1010
 35. Balasubramanian, S., Kanade, S., Han, B., and Eckert, R. L. (2012) A proteasome inhibitor-stimulated Nrf1 protein-dependent compensatory increase in proteasome subunit gene expression reduces polycomb group protein level. *J. Biol. Chem.* **287**, 36179–36189
 36. Marshall, R. S., McLoughlin, F., and Vierstra, R. D. (2016) Autophagic Turnover of Inactive 26S Proteasomes in Yeast Is Directed by the Ubiquitin Receptor Cue5 and the Hsp42 Chaperone. *Cell Reports* **16**, 1717–1732
 37. Salazar, A., Keusgen, M., and von Hagen, J. (2016) Amino acids in the cultivation of mammalian cells. *Amino Acids* **48**, 1161–1171
 38. Yamamoto, K., and Niwa, A. (1993) Amino acid and vitamin requirements in mammalian cultured cells. *Amino Acids* **5**, 1–16
 39. Vizcaino, J. A., Csordas, A., del-Toro, N., Dianes, J. A., Griss, J., Lavidas, I., Mayer, G., Perez-Riverol, Y., Reisinger, F., Ternent, T., Xu, Q. W., Wang, R., and Hermjakob, H. (2016) 2016 update of the PRIDE database and its related tools. *Nucleic Acids Res.* **44**, D447–D456